J Mater Sci: Mater Electron (2022) 33:7275–7287

Structural, optical, and electrical characterizations of Cr-doped CuO thin films

Silan Baturay[1], Ilhan Candan[1,2,*], and Cihat Ozaydın[3]

[1] *Department of Physics, Faculty of Science, Dicle University, 21280 Diyarbakir, Turkey*
[2] *Department of Physics, Institute of Science and Technology, Dicle University, 21280 Diyarbakir, Turkey*
[3] *Department of Computer Engineering, Faculty of Engineering, University of Batman, 72100 Batman, Turkey*

Received: 27 November 2021
Accepted: 5 February 2022
Published online:
16 February 2022

© The Author(s), under exclusive licence to Springer Science+Business Media, LLC, part of Springer Nature 2022

ABSTRACT

The polycrystalline copper oxide (CuO) thin films have been produced using the method of spin coating on the soda–lime glass (SLG) as well as the substrate of p-type Si (1 0 0) wafers at 500 °C in furnace. The obtained undoped and Cr-doped thin films of CuO have been comprehensively characterized via X-ray diffraction (XRD), ultraviolet–vis (UV–Vis) spectroscopy, the current–voltage (*I*–*V*), and capacitance–voltage (*C*–*V*) characteristics for providing information on quality of the crystalline nature, change in energy band gap and electrical properties, respectively. Structural analysis results obtained from XRD data demonstrate that CuO films in conjunction with Cr doping indicated that all thin films have monoclinic polycrystalline nature, with two main peaks of (− 111) and (111) with d_{hkl} of about 2.52 and 2.32 Å, respectively. The transmittance and energy band gap values of undoped and Cr-doped thin films of CuO ranging in varying concentration ratio have been determined in the wavelength region of 300–1100 nm. The highest value has been found to be around 33% related to 3% Cr doping in the visible range. UV–Vis spectrum analysis results indicate that both transmittance value and energy band gap value of the CuO films are changed with the increase in Cr doping ratio in CuO solution at room temperature. The band gap energy was determined to be between 1.67 and 2.03 eV with the increase in Cr concentration. The *I*–*V* and *C*–*V* characteristics of Cr:CuO/p-Si diodes were associated with the CuO/p-Si diodes. Although the best rectification ratio (*RR*) is seen in the 1% Cr-doped diode ($RR = 2.33 \times 10^3$ for ± 1 V), other diodes also have significant rectification behavior. It is seen that doping of Cr had a significant change on the obtained devices' performance. Thus, the Cr:CuO/p-Si diodes generated by 1% Cr doping using spin coating method had the highest light sensitivity compared with those of the other diodes.

Address correspondence to E-mail: ilhan.candan@dicle.edu.tr

https://doi.org/10.1007/s10854-022-07918-2

1 Introduction

The metal–oxide nanostructures' extraordinary properties and structural difference started wide-ranging research focus in various nanoscale fields including electronics, catalysis, optics, optoelectronics, electrodes in lithium-ion batteries, gas sensors, and biosensors [1–7]. As a metal oxide semiconductor, CuO nanofilms are a major interest between other kinds of the metal oxide semiconductor. Because of the material's stability, non-toxicity, and low cost of production, recently a great attention is focused on the nanostructured forms of copper oxides [8, 9]. Copper oxide should be classified into two different stable forms which are known as cupric oxide (CuO) and cuprous oxide (Cu_2O). CuO with nanostructures having semiconductor material of p-type conductivity exhibits intriguing properties such as direct energy band gap value (between 1.1 and 2.1 eV) [10, 11], environmentally friendly and unique chemical stability, in contrast, Cu_2O has cubic structure that has 2–2.6 eV energy band gap with black color [12]. CuO as a semiconductor candidate is very promising for various application areas including H_2 gas sensors [13], CO_2 sensor [14], cross-point memory [15], solar selective absorber [16], solar cell [17], photoelectrochemical applications [18], perovskite solar cells [19], and electrochemical supercapacitors [20] owing to abundant availability in nature and low-cost synthesis and easy preparation process of copper production [21, 22]. It should be noted that CuO has been both direct [23] and indirect energy band gap values [24] which are more than cuprous oxide compound, and fabrication methods strongly effect these values. Kuhaili indicated that cupric oxide for temperatures only below 300 °C is the stable phase at different partial pressures of oxygen ($P(O_2)$), and merely less than 1000 °C for atmospheric pressure, the equilibrium phase diagram of the Copper–Oxygen (Cu–O) system [25]. Otherwise, cuprous oxide is thermodynamically stable only in $P(O_2)$ range of temperature, and that is obtained by heating of Cu with $P(O_2)$ below 10 mTorr using a KrF excimer laser (248 nm) above 650 °C [26]. Nevertheless, nanocrystalline Cu_2O phase was additionally seen by annealing thin films of Cu in air at temperatures less than 300 °C [27, 28]. A single monoclinic CuO phase was also obtained from the films annealed tubular furnace with some increment in the healing temperature such as between 350 and 450 °C in air condition [27]. The research on CuO thin films has attracted extensive interest because of the fact that the p-type conducting oxide development [20] has significant importance in technology for p–n homo-junction-based oxide materials. Moreover, metal–semiconductor (MS) and metal–interlayer–semiconductor (MIS)-type Schottky diodes' electrical properties started considerable interest in experimental studies owing to metal and semiconductor interlayer's different optical and electrical properties [29, 30]. Since these devices' performance and reliability are particularly based on the interlayer formation, they effect parameters including the barrier height, interface-state density, series resistance as well as ideality factor.

Surface morphology, donor density, surface charge, oxygen vacancies' presence, and its catalytic effects in CuO can be significantly enhanced with doping of Cr [7, 31]. Doping of Cr is preferred for the semiconductor materials owing to the fact that the CuO material's properties can be significantly changed by the doping of Cr such as NH_3 sensing, transmittance value, and optical bang gap [32–34]. Various methods have been used to fabricate CuO and Cu_2O thin films with dissimilar morphology. Monoclinic CuO and cubic Cu_2O thin films could be manufactured via copper's thermal oxidation at 250 and 350 °C in the air, respectively [35]. Samarasekara et al. fabricated thin films of CuO using sol–gel spin coating technique and investigated Zn^{2+}-doped CuO thin films' electrical properties. They found that Zn^{2+}-doped CuO films indicate electrochemical cell behavior only after illumination [36]. Guillen and Herrero fabricated thin films of Cu_2O and CuO via low-temperature oxidation processes and found that there is one level in the energy band gap of CuO which was attributed to the oxygen's mono-vacancies and two defect levels next to the Cu_2O conduction band owing to vacancy complexes and mono-vacancies [35]. Shaban et al. employed spincoating technique to investigate phase mixed with Cu_2O/CuO structural, optical, and gas-sensing properties and they found that the sensitivity of 6% Cr and 3% S doping of Cu_2O/CuO thin films significantly improved from 46 to 99.8% towards the flow rate of Co_2 which increased from 30 to 150 sccm [37]. Pat et al. [2] deposited Cu_xO thin film with Cr doping via technique of thermionic vacuum arc plasma and they had high transparency and dielectric constant [38]. Even though CuO-based materials have been

researched for the characteristics of dark *I*–*V* [39–41], response of photocurrent [42–44], and gas molecules' sensitivity [11, 12, 40, 45], comprehensive realization on the device characteristics such as diode parameters and carrier transport mechanisms' domination have yet not been accomplished.

Recently, transition metal oxides have been deposited [41, 46–49] to improve the crystalline nature of CuO thin films. Though different doped CuO thin films' physical and chemical properties have been examined by groups [21, 50–53], CuO thin films with Cr doping are very limited in the literature. For all these reasons, Cr-doped CuO thin films' further investigation on structural, morphological, optical, and electrical properties will contribute to the limited available literature.

In the present study, CuO thin films with Cr doping were obtained by spin coating technique that is conventional, environmentally friendly, and suitable for our research. The CuO thin films' structural, morphological, optical, and electrical properties were investigated. The thin films are fabricated on glass and substrates of p-Si. The obtained Cr-doped films' structural and optical properties have been investigated by employing XRD and UV–Vis spectroscopy, respectively, for providing data on the crystalline nature's quality and surface morphology change of the obtained films. Additionally, we have investigated the diodes' electrical properties to analyze the concentration effect on diode parameters of Cr:CuO/p-Si diodes by employing the measurements of current–voltage (*I*–*V*) and capacitance–voltage (*C*–*V*) in the dark and light (100 mW/cm^2).

2 Experimental

Cr-doped CuO thin films with Cr/Cu ratios of 0, 1, 2, and 3% were prepared using spin coating method as well as SLG and wafers of p-type Si (1 0 0) as substrate that have 1–10 Ω-cm resistivity. Before deposition process, SLG substrates were firstly boiled in 5:1:1 deionized water, ammonia, and hydrogen peroxide mix for a time of 20 min. at a temperature of 90 °C and in the solution of 5:1:1 deionized water, hydrogen peroxide, and hydrogen chloride with the same conditions. The purpose of these cleaning steps is to remove the unnecessary impurities on the substrate. Then, the substrates were cleaned in acetone for 5 min. each for two times to obtain a clearer surface. After this process, the substrates further cleaned by distilled water and dried under N_2 gas, respectively. Then, the Si wafers to obtain Cr:CuO/p-Si diode were boiled for 5 min. in trichloroethylene, and later, stirred for 5 min in acetone each for two times and ethanol to obtain free of any organic contamination in ultrasonic bath. The wafers were etched in hydrofluoric acid (HF) solution:distilled water (H_2O) (1:10) two times for 30 s and then, washed by distilled water to eliminate the native oxide and any chemical residues before inserting them into the vacuum chamber to obtain Cr:CuO/p-Si diode. The rear contacts were made by evaporating an Al metal of 200 nm thickness on the Si wafers' unprocessed side, and that was continued by a speedy thermal annealing for 3 min. at 570 °C under a N_2 gas.

A 0.1 M copper(II) acetate ($Cu(CH_3COO)_2 \cdot H_2O$) in ethanol solution was employed as the preliminary material and a 0.01 M solution of chromium(III) chloride ($CrCl_3 \cdot 6H_2O$) in ethanol was used as the dopant source, respectively. The obtained solutions were firstly deposited on p-Si wafer with (100) orientation by spin coating method at 1500 rpm for 55 s for three layers of deposition. After this, the obtained films were annealed for 1 h in a furnace at 500 °C under air. Lastly, front contacts of Al were vaporized onto the Cr-doped CuO thin films employing a shadow mask for investigating the heterojunctions' electrical properties. Then, the obtained solutions were placed on the substrates of SLG using the forementioned technique and conditions for ten layers of deposition to investigate the Cr-doped CuO thin films' structural and optical properties. During deposition process, each layer of the films was preheated to 230 °C on a hot plate for 10 min to obtain a homogenous surface.

The undoped and Cr-doped CuO thin films' structural and phase purity analysis were determined by a Rigaku ultima III diffractometer operated by CuKα radiation source with wavelength of 0.154 nm at 40 kV, and 30 mA for θ–2θ range in the steps of 0.02° (θ) from 20° to 80° at room temperature. The conclusion of thin films' transmittance and energy band gap was analyzed by UV–Vis spectrophotometer for the wavelength range between 300 and 1100 nm. *I*–*V* relations of all films were inspected by a source meter (Keithley 2400, Cleveland, USA) both in dark and under illumination with light of 100 mW/cm^2 at room temperature to investigate the change of barrier height and ideality factor.

3 Structural properties

The prepared Cr-doped CuO thin films' structural analysis was investigated by X-Ray diffraction. The obtained samples' XRD patterns are displayed in Fig. 1. The positions of peaks at 2θ angle that are around 35.6°, 38.8°, 48.8°, 53.5°, 66.41°, and 68.07°, with d_{hkl} around 2.52, 2.32, 1.86, 1.71, 1.41, and 1.38 Å were related to (JCPDS 05-6661 for CuO) (– 111), (111), (– 202), (020), (– 311), and (113) reflections planes, respectively. According to the XRD data, it is said that the samples' XRD patterns show a CuO single phase's existence with a monoclinic structure [1–3]. There are no signs of oxide phases associated with the impurity phase owing to the formation of the possible compounds containing chromium oxides and Cu_2O.

The diffraction data obtained from XRD including the values of peak orientations, strain (ε), grain sizes (D), dislocation density (δ), inter-planar spacing (d-spacing), and full width at half maximum (FWHM) for the strong peaks are given in Table 1. The intensities of peaks and full width at half maximum values which were employed to determine the grain size slightly change with the increase in Cr concentration. Cr addition in the samples in air at temperature at 500 °C change the composition and the crystal structure of the thin film; and also the peak intensities and orientation along (– 111) and (111) were higher. It is said that Cu ions' exchange changes the structure of crystal or crystallinity slightly owing to the fact that it is probably related to the Cr^{+} ion's atomic radius (0.62 Å) being smaller than Cu^{2+} ions' one (0.73 Å). When the results were compared with the previous studies, it was concluded that the given planes' orientation and intensity for CuO thin films mostly approve a strong crystallinity with monoclinic structure [4]. Das and Alford revealed that the Ag-doped CuO thin film had preferential orientation along the line in (111) [5]. Menazea and Ayman indicated similar results and they showed that it had a preferential orientation in the (200) direction [6]. Obulapathi et al. [54] indicated similar XRD data. They indicated that the intensity of the peaks changed by the addition Cr into the CuO thin films.

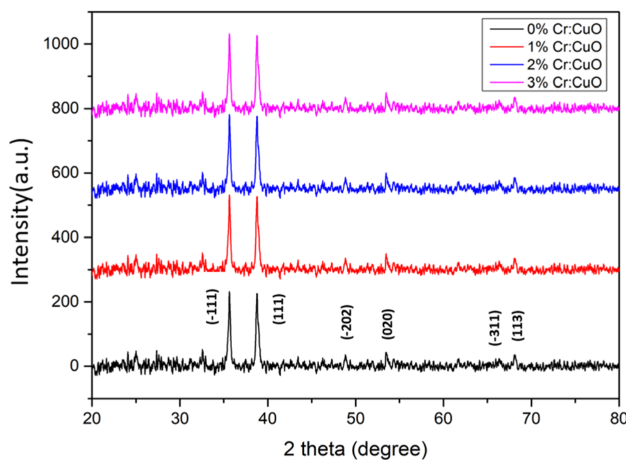

Fig. 1 XRD patterns of CuO thin films with Cr doping

Cr-doped CuO thin film's crystallite size (D) was determined by the angular peak width at FWHM of (– 111) and (111) planes by employing the following expression [55]:

$$D = \frac{0.94\lambda}{\beta \cos\theta}, \quad (1)$$

where λ is 1.5418 Å as the XRD wavelength, θ is the angle of Bragg diffraction, β is the angular peak width at FWHM, and D is the crystallite size of the film of (– 111) and (111) planes. Calculation from X-ray diffraction data showed a change in the crystallite size as a function of the Cr concentration. The calculation of Cr-doped CuO thin films' crystallite size shows a change in D value as a Cr doping function at a 500 °C constant annealing temperature. Durai et al. [56] showed that the D value of the Cr-doped CuO changes owing to a rise in absorbed atoms' mobility. d values of the obtained CuO film are determined by the Bragg's expression [46]:

$$2d\sin\theta = n\lambda, \quad (2)$$

where n is the diffraction order. Calculated d values of undoped and CuO thin films with Cr doping for (– 111) and (111) are around 2.52 and 2.32, respectively. The value of dislocation density (δ) that shows the defects' amount in samples is calculated using the formula [46]:

$$\delta = \frac{1}{D^2}. \quad (3)$$

The change in the strain of the all films is determined using the following expression [27]:

$$\varepsilon = \frac{\beta}{4\tan\theta}. \quad (4)$$

The dislocation density value is changed between 56.87×10^{13} and 83.47×10^{13} m^{-2} for (– 111) plane and 13.88×10^{13} and 17.19×10^{13} m^{-2} for (111)

Table 1 Crystallite size, dislocation density, and strain value of the undoped and Cr-doped CuO films obtained by XRD

	Theta peaks (θ)	Grain size (nm)	*d*-spacing (Å) (calculated)	*d*-spacing (Å) (standart)	Orientation	Dislocation density ($\times$ 10^{15} m^{-2})	Strain
Undoped	35.63	27.35	2.52	2.520	(− 111)	1.34	0.25
	38.79	19.61	2.32	2.319	(111)	2.60	0.32
1% Cr-doped	35.64	19.25	2.52	2.519	(− 111)	2.70	0.35
	38.77	26.20	2.32	2.323	(111)	1.46	0.24
2% Cr-doped	35.64	25.73	2.52	2.521	(− 111)	1.51	0.26
	38.78	20.10	2.32	2.323	(111)	2.48	0.31
3% Cr-doped	35.65	16.94	2.52	2.519	(− 111)	3.49	0.40
	38.77	15.31	2.32	2.323	(111)	4.27	0.41

plane owing to the fact that the δ values are inversely proportional to the D value squared. Strain values of the (002) and (111) planes are changed with Cr dopant content. Therefore, it was said that the main effect of change in D is linked to change in strain. Durai et al. [56] showed that Cr-doped CuO films as function of concentration show a change in strain value owing to strain relaxation with changed D value.

4 Optical properties

The optical properties including absorbance, transmittance, and band gap of undoped and CuO thin films with Cr doping via spin coating method were analyzed in detail to examine the Cr doping effect using UV–visible spectrophotometer data in the range of 300–1100 nm. The absorption coefficient and the undoped and Cr-doped CuO thin films' optical transmission spectra for four different doping concentration deposited on SLG substrate are given in Figs. 2 and 3, respectively. It was found that the CuO thin films' optical transmittance values increase in visible region as compared to undoped CuO film and the highest value has been found to be around 33% related to 3% Cr doping in the visible range. This result could be used to improve the efficiency of photovoltaic devices. This upsurge in the value of optical transmittance is assigned to the crystalline nature of the thin film characteristics because these changes are corresponding to the material properties of the thin films. The rise in the transmittance value of obtained CuO thin film could be ascribed to the Moss–Burstein (M–B) effect [57]. Thus, it is said that the CuO thin films' optical properties can be changed by Cr dopant content in the ultraviolet–visible range (401–750 nm) of the optical spectrum from 300 to

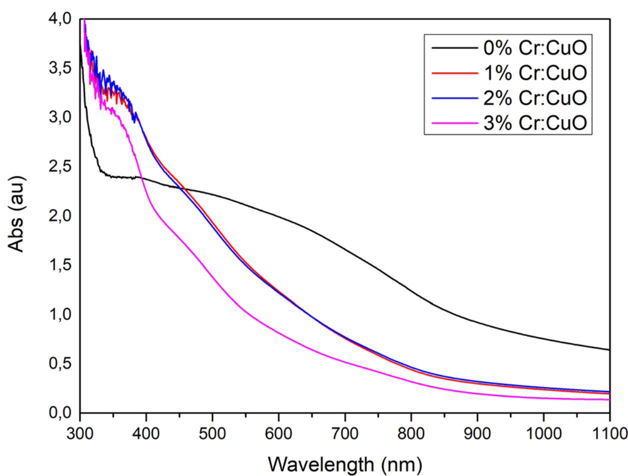

Fig. 2 Absorbance spectrum of CuO thin films for different Cr concentrations

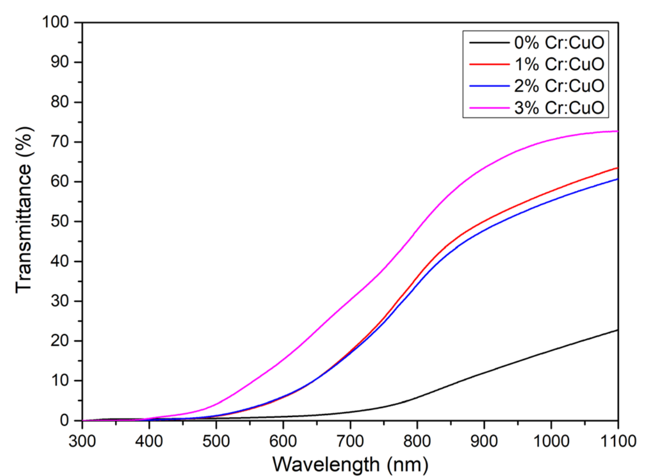

Fig. 3 Transmittance spectrum of CuO thin films for different Cr concentrations

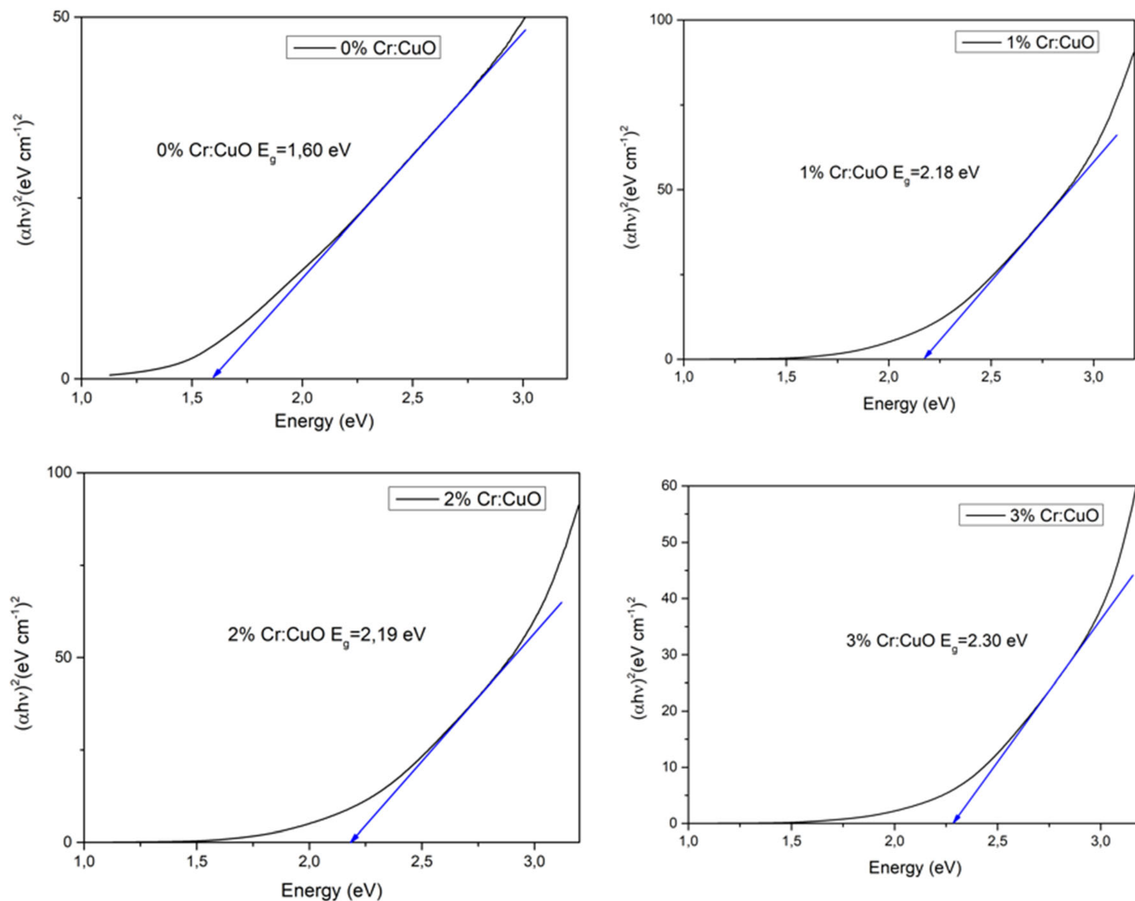

Fig. 4 $(\alpha h\nu)^2$ vs. $h\nu$ plot of Cr-doped CuO thin film on soda–lime glass substrate

1100 nm. Thus, it is said that the optical properties including transmittance and absorbance of CuO thin films can be changed by different Cr dopant contents in the ultraviolet–visible range region. The change in values of absorbance and transmittance indicates that CuO thin films could be applied to numerous applications including photovoltaic devices [58]. Menazea and Mostafa [59] revealed that the CuO thin films' optical transmittance value is improved with Ag doping using Laser Deposition (PLD) technique. They also said that the enhancing in the transmittance value may be allocated to the structural properties of the prepared thin films.

The increase of the value of transmittance corresponds to change of the energy band gap corresponding to valence and conduction electrons. The direct energy band gap values of the all thin films are calculated via the Tauc's expression as follows [60]:

$$\alpha h\upsilon = A\left(h\upsilon - E_g\right)^m, \quad (5)$$

where $h\upsilon$ is the radiation energy, E_g is the band gap of the used materials, A is the material's energy independent constant, n is constant that is based on the transition nature, $m = 1/2, 2, 3/2$, or 3 for direct, non-direct allowed transition, forbidden direct or forbidden non-direct transitions, respectively. In our case, the transition is direct and $m = 1/2$. α is a constant that gives the coefficient of absorption in cm^{-1} which is also calculated using the equation; $\alpha = 4\pi k/\lambda$ [61]; k is the absorption index of material and λ is the wavelength. Figure 4 indicates the plot of $(\alpha h\nu)^2$ versus incident energy of photon ($h\nu$) for undoped and Cr-doped CuO films. Undoped CuO thin film's calculated band gap value is 1.60 eV, which increases to 2.30 eV after the doped by Cr in solution. The Cr-doped CuO thin films reveal both high transmittance as well as maximum energy band gap among the obtained thin films. Gülen et al. indicated that the value of energy band gap was improved with Mn doping concentration in the thin film using SILAR method [62]. Pat et al. [38] revealed that energy band

gap value of the Cr-doped Cu_xO thin film was measured to be around 2 eV using thermionic vacuum arc plasma. Sajid et al. [63] indicated that the pure CuO thin films' energy band gap is calculated to be 1.87 eV that is greater than bulk CuO (1.2 eV) because of confinement effects at quantum nanoscale level. Also they show that CuO thin film's energy band gap value has been increased up to 2.61 eV conjunction with Cr doping owing to the effects of band-filling as well as s–d and p–d exchange interactions. Das and Mitra [64] revealed that increase in energy band gap in doped films was seen up to 6% doping level owing to the increase in carrier density in Ni-doped CuO films.

It is said that the increase in Cr concentration causes the evaporation of oxygen and the obtained films become more Cu rich owing to the fact that the O-rich samples usually have lower energy band gap value [65, 66]. Relatively more Cu-rich thin films after Cr doping owing to the evaporation of excess oxygen from the film surface will have an increase in the value of energy band gap as compared to the undoped CuO film. It is said that the change in the energy band gap conjunction with Cr doping might be capable for the effect of band-filling. Thus, it is said that Cr could be used to regulate the CuO thin films' optical band gap for potential electronic devices.

5 The current–voltage and capacitance–voltage characteristics of the Cr:CuO/p-Si diodes

To evaluate the fabricated heterojunction diodes' electrical properties, semi-logarithmic *I*–*V* plots were drawn from current–voltage measurements in the dark and under light (100 mW/cm^2). All diodes' *I*–*V* characteristics in the dark are shown in Fig. 5.

As seen in Fig. 5, although the best rectification ratio (*RR*) is seen in the 1% Cr-doped diode (*RR* = 2.33 × 10^3 for ± 1 V), other diodes also have significant rectification behavior. At relatively low voltages, the Cr:CuO/p-Si heterojunction acts like a Schottky barrier diode [67]. Therefore, the Cr:CuO/p-Si diodes' *I*–*V* characteristics are explained by theory of Thermionic Emission (TE) which is well known and stated in the following equations [68–70]:

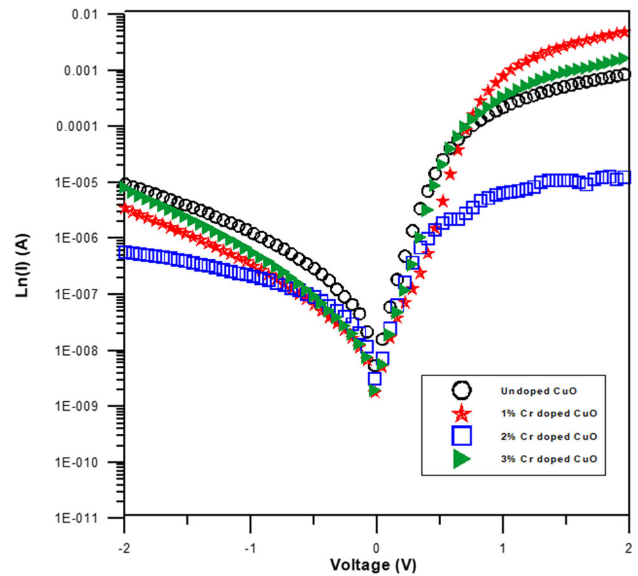

Fig. 5 Semi-logarithmic *I*–*V* plots of the Cr:CuO diodes in dark

$$I = I_0 \exp\left(\frac{qV}{nkT}\right)\left[1 - \exp\left(-\frac{qV}{kT}\right)\right], \quad (6)$$

where V is the applied voltage, n is the ideality factor, k is the Boltzmann constant, T is the absolute temperature in Kelvin, and I_0 is the saturation current which is given by [71, 72]

$$I_0 = AA^* T^2 \exp\left(\frac{-q\phi_b}{kT}\right), \quad (7)$$

where A is the diode area (7.85 × 10^{-3} cm^2), A^* is the effective Richardson constant and equal to 32 Acm^{-2} K^{-2} for p-type Si, q is the electron charge, and ϕ_b is the barrier height. The ideality factor n is related to the diode's conformity in the TE theory, and it is calculated from the linear region's slope of the forward bias in the plot of ln(I) − V characteristics via the following relation (for $V \geq 3kT/q$) [73]:

$$n = \frac{q}{kT}\left(\frac{dV}{d\ln I}\right). \quad (8)$$

The diode parameters n, ϕ_b, I_0 , and RR are determined from the experimental *I*–*V* data at 300 K temperature and are given in Table 2. The results show that %1 Cr doping to CuO causes a slight improvement in the ideality factor. However, all the produced diodes' ideality factors are higher than unity, indicating that they demonstrate the behavior of non-ideal diode. Ideality factors' higher values are associated to secondary mechanisms that involve dipoles of interface because of doped interface or

Table 2 The electrical parameters of Cr:CuO/p-Si diodes with different doping ratios (0%, 1%, 2%, and 3%) at 300 K and dark conditions

Sample	n	ϕ_b (I–V) (eV)	I_0 (A)	RR (for ± 1 V)	$\phi_{b(\mathrm{Norde})}$ (eV)	R_s (kΩ) (Norde)
0%Cr:CuO/p-Si	2.28	0.73	1.16×10^{-8}	170.7	0.791	4.173
1%Cr:CuO/p-Si	2.17	0.81	4.55×10^{-10}	2335.4	0.734	0.312
2%Cr:CuO/p-Si	2.47	0.75	5.26×10^{-9}	30.4	0.803	36.74
3%Cr:CuO/p-Si	2.14	0.77	2.22×10^{-9}	557.2	0.859	1.064

structure of specific interface, and also defects of fabrication at the interface [74]. Furthermore, n's large values may also be related to a wide distribution of low Schottky barrier patches due to the laterally inhomogeneous barrier [75]. Erdoğan and Güllü [74] calculated the ideality factor and barrier height being as 2.39 and 0.64 eV, respectively, for the Au/CuO/p-Si diode they constructed by the simple chemical method. Similarly, Ruzgar et al. [76] reported Au/(CuO:La)/n-Si photodiode's electrical performance that is formed with undoped CuO and La-doped CuO thin films produced by spin coating method. They calculated the best ideality value as 2.04 with 2% La doping CuO.

Another important parameter for Schottky barrier diodes is the barrier height (ϕ_b). Akin to the improving the diodes' ideality factor values, the height of barrier becomes optimum and maximum value reaching to 0.81 eV with 1% Cr doping. The 0.81 eV ϕ_b value we attained for the Al/%2Cr:CuO/p-Si device is considerably higher than both the barrier heights of the other diodes and the conventional MS contact diode's value such as the Al/p-Si diode, where ϕ_b is approximately 0.70 eV [77]. Some researches have experimentally been carried out for the modification of barrier employing the thin films' interlayer [76]. Recently, Ruzgar et al. [8] have published a paper about the Au/Fe:CuO/n-Si diode made by doping Fe to CuO. They reported that the barrier height changed with Fe doping to CuO and that the barrier height decreased as Fe doping increased. Similarly, Singh et al. [78] obtained 2.8 ideality factor and 0.82 eV barrier height for the n-CuO/p-Si diode, which they formed by method of sol–gel spin coating. In another study, Ruzgar et al. [76] stated that the height of barrier was the highest and optimum when the La contribution was 2% for the Au/La:CuO/n-Si diodes obtained by doping 2, 5, and 10% La to CuO. Based on these, we can state that doping changes the barrier height of the diode and that the highest and optimum barrier height is achieved with 1% initial Cr doping to CuO in our work. The I–V graphs shown in Fig. 5 deviate from linearity having relatively large forward biases associated with the effects of series resistance. The diodes' series resistance can be investigated using Norde's method [79]. This includes a modified Norde function, and the function $F(V)$ is expressed as [80]

$$F(V) = \frac{V}{\gamma} + \frac{kT}{q}\ln\left(\frac{I(V)}{A^{*}AT^{2}}\right), \tag{9}$$

where γ is a dimensionless arbitrary integer larger than idealty factor n and $I(V)$ is the diode's current in region of forward bias.

Figure 6 shows the Cr:CuO/p-Si diodes' $F(V)$–V graph for a few different concentrations of Cr doping. According to the Norde's method, the values of barrier height ϕ_b and series resistance R_s are expressed by the equations as follows [79, 81]:

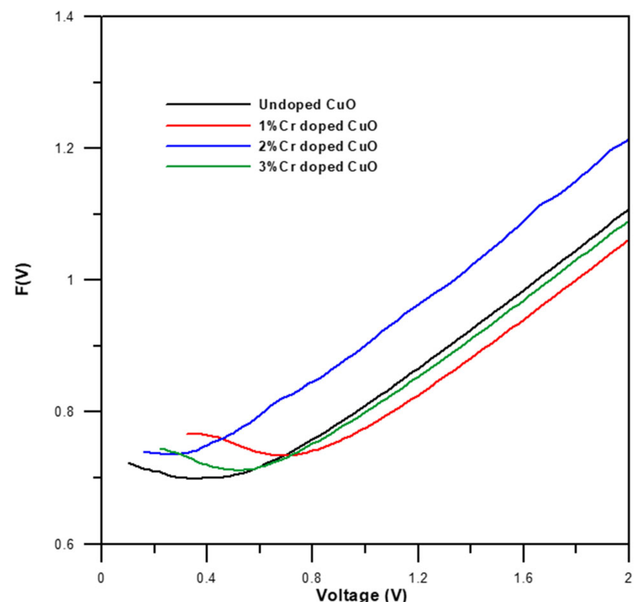

Fig. 6 Norde plots of the CuO/p-Si and Cr:CuO/p-Si heterojunctions

$$\phi_b = F(V_0) + \frac{V_0}{\gamma} - \frac{kT}{q} \quad (10)$$

$$R_s = \frac{kT(\gamma - n)}{I_0}, \quad (11)$$

where $F(V_0)$ is the $F(V)$'s minimum point, V_0 and I_0 are voltage and current corresponding to this point, respectively. ϕ_b and R_s values calculated by Norde's method are given in Table 1. From the results, diode of 2% Cr:CuO/p-Si exhibited the largest series resistance with 3674 kΩ, while diode of 1% Cr:CuO/p-Si showed the smallest series resistance. The obtained ϕ_b values from the experimental I–V data and calculated from the Norde's expression have similar variation inclination but marginally different. This difference is generally associated with barrier inhomogeneity and the non-linear behavior of diode [74, 76].

To evaluate the Cr doping effect on the CuO-based diodes' photoelectric properties, the diodes' I–V measurements in the dark and under light were taken and their plots are shown in Fig. 7a–d.

As can be seen from Fig. 7a–d, the currents of all diodes under illumination are higher than currents in dark. However, when compared with the most of other diodes, the high light sensitivity was realized in the diode with 1% Cr doping. Overall, illumination does not significantly change the forward bias currents, whereas the reverse bias current changed significantly with illumination. Higher energy photons compared with the materials' optical band gap energies that make up the diode provide electron–hole pairs. Since these photogenerated carriers contribute more to the current carriers in the reverse bias region, a significant increase in current occurs in this region. Thus, the diodes produced exhibit the typical photosensitive property. Table 3 demonstrates the ratio of diodes' dark and illuminated reverse bias currents (at − 2 V), open circuit voltage (V_{OC}), and short circuit current (I_{SC}).

For Schottky heterojunction diodes, measurements of capacitance are an important non-destructive technique to obtain information on constant charge concentration and barrier height. Figure 8 illustrates the %1 Cr:CuO/p-Si heterojunctions' C–V measurements at different frequencies (10 kHz–1 MHz) at 300 K in dark. As can be seen in Fig. 8, the C–V plot gives peaks around 1 V for each frequency, the value of which decreases with frequency. This is related to the behavior of interface states. When the frequency increases, the interface loads in the traps cannot follow the AC signal [82].

The capacitance values of the %1 Cr:CuO/p-Si diode decrease with the increase in frequency as given in Fig. 8. In general, the reverse bias voltage and frequency strongly effect the capacitance measurement in the Schottky diode. The capacitance's dependence on voltage and frequency is due to certain properties of the heterojunction, such as interface states, pollution level, series resistance as well as layer interface between Cr:CuO and p-Si [83]. The capacitance's higher values at low frequencies may be associated with the interface states' continuous distribution and depletion capacitance of the diode [84]. On the other hand, charge carriers of high frequencies in the interface cannot contribute to the capacitance as they cannot track the signal of alternating current. As a result, the diode's capacitance value has a tendency to be the same while the frequency rises [85]. The a diode's depletion region capacitance is expressed as [86]

$$\frac{1}{C^2} = \frac{2(V_{bi} + V)}{q\varepsilon_s A^2 N_a}, \quad (12)$$

where A is the area of diode, V is the voltage of reverse bias, V_{bi} is the diffusion potential at zero bias and obtained from the C^{-2}–V plot's extrapolation to the axis of V, where ε_s is the the semiconductor's ($11.8\varepsilon_0$ for p-Si) dielectric constant, N_a is the p-type semiconductor's acceptor concentration.

Figure 9 demonstrates the C^2–V and C–V graphs of a 1% Cr:CuO/p-Si heterojunction diode at 1 MHz and temperature of 300 K. The values of V_{bi} and N_a were found to be 0.59 eV and 3.618×10^{16} cm^{-3}, respectively. The height of barrier could be determined employing the C–V data by the expression as follows:

$$\phi_{b(C-V)} = V_{bi} + \frac{kT}{q} \ln\left(\frac{N_v}{N_a}\right), \quad (13)$$

where N_v is the valance band states' effective density for p-Si (N_v = 3.2×10^{19} cm^{-3}) [7]. The 1% Cr:CuO diode's barrier height was calculated as 0.765 eV from the measurement of C–V. The diode's barrier height values attained from the I–V and C–V measurements are close. However, the values acquired by both methods are slightly different. This can also be described by the I–V and C–V measurements'

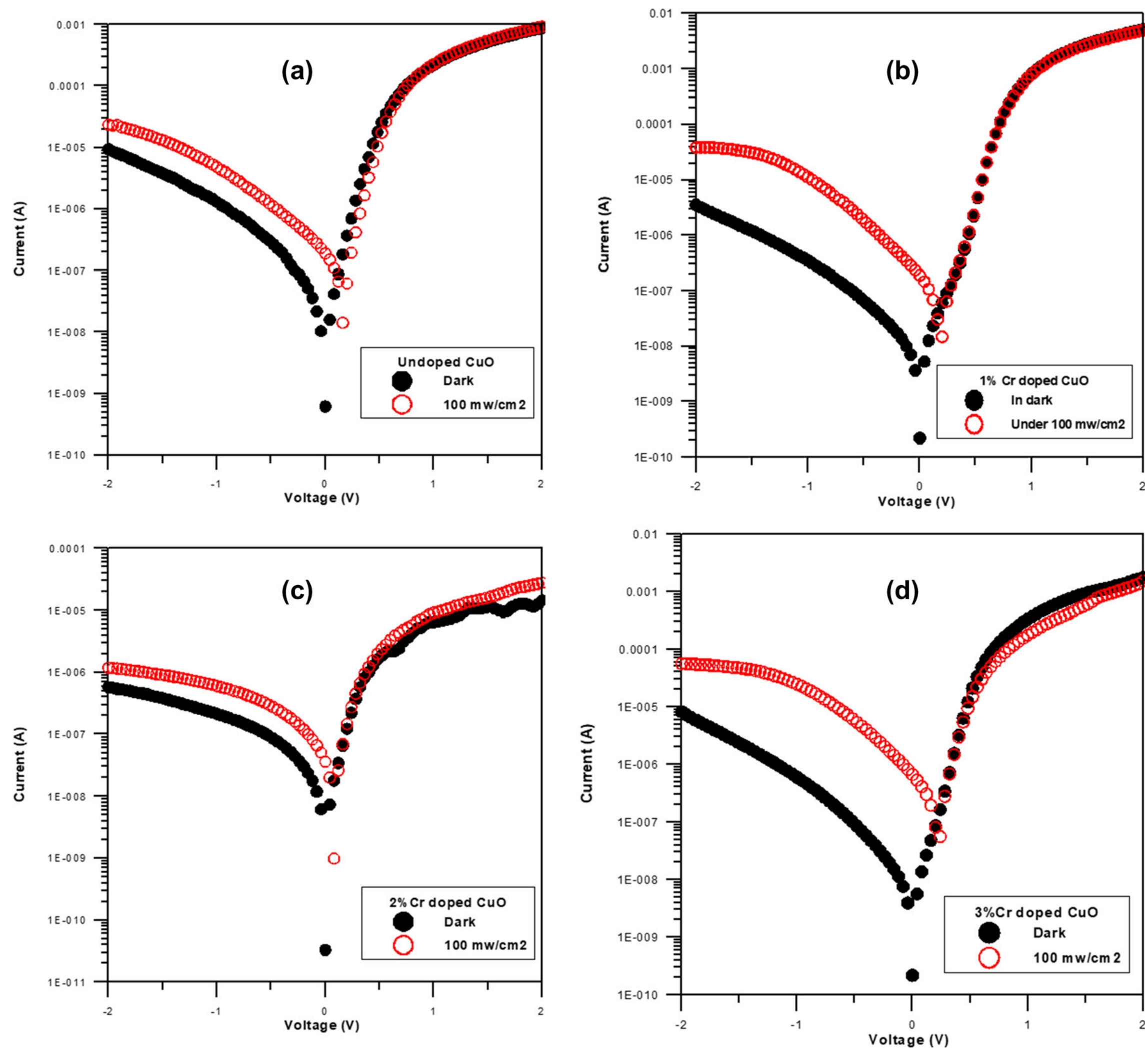

Fig. 7 **a–d** ln I–V plots of the CuO/p-Si and Cr:CuO/p-Si heterojunctions in the dark and under light (100 mW/cm^2)

Table 3 Photoelectrical parameters of CuO/p-Si and Cr:CuO/p-Si diodes under illumination with 100 mW/cm^2 light

Diode	Photosensitivity ratio	V_{OC} (mV)	I_{SC} (µA)
CuO/p-Si	3.30	160	0.190
1% Cr-doped CuO/p-Si	33.74	180	0.191
2% Cr-doped CuO/p-Si	2.06	80	0.036
3% Cr-doped CuO/p-Si	27.82	220	0.663

different nature and the presence of semiconductor's interfacial layer as well as trap states [73, 80].

6 Conclusion

In summary, Cr-doped CuO thin films were grown on SLG substrate, and CuO/p-Si as well as Cr:CuO/p-Si structures were produced by depositing thin films on p-type Si wafers using method of spin coating and annealed at 500 °C for 1 h in air condition. The Cr doping effect on structural, optical, morphological, and electrical properties of these films was comprehensively explored. The CuO films conjunction with Cr doping were monoclinic polycrystalline structure and with two main peaks (− 111) and (111) with d_{hkl} about 2.52 Å and 2.32 Å, respectively. The obtained thin film's XRD parameters

including crystallite size, dislocation density, and strain slightly changed with the increase in Cr concentration. The thin film's transmittance value was increased in the visible range as compared to undoped CuO thin film. The highest value has been found to be around 33% related to 3% Cr doping in the visible range. The band gap energy was determined to be between 1.67 and 2.03 eV with the increase in Cr concentration. The energy band gap was radically increased with an increase of Cr concentration in CuO. Additionally, CuO/p-Si and Cr:CuO/p-Si structures were obtained by depositing thin films on p-type Si wafers via method of spin coating. The devices' electrical properties were analyzed in detail using *I*–*V* measurement in the dark and under illumination employing a solar simulator. The results show that %1 Cr doping to CuO causes a slight improvement in the ideality factor. *C*–*V* measurements were carried out in the dark with a frequency range of 1–500 Hz. The 1% Cr:CuO diode's barrier height was calculated as 0.765 eV from the measurement of *C*–*V*. The results reveals that Cr doping significantly altered the devices' electrical and photoelectrical parameters. The highest height of barrier, largest V_{OC} and I_{SC} were determined to be in 3% Cr-doped CuO thin films. Moreover, the structures formed using 3% Cr-doped CuO films exhibited the smallest ideality factor and series resistance. Thus, the obtained thin film's parameters could be employed for photovoltaic devices on the future studies.

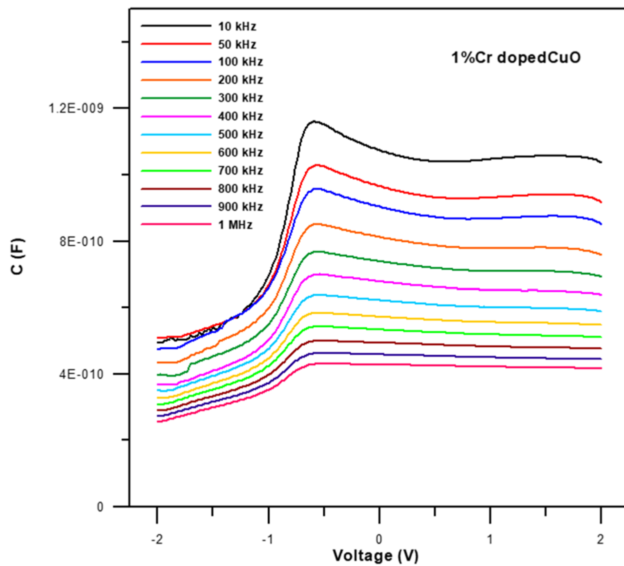

Fig. 8 The *C*–*V* measurements of the 1% Cr:CuO/p-Si heterojunctions at different frequencies (10 kHz–1 MHz)

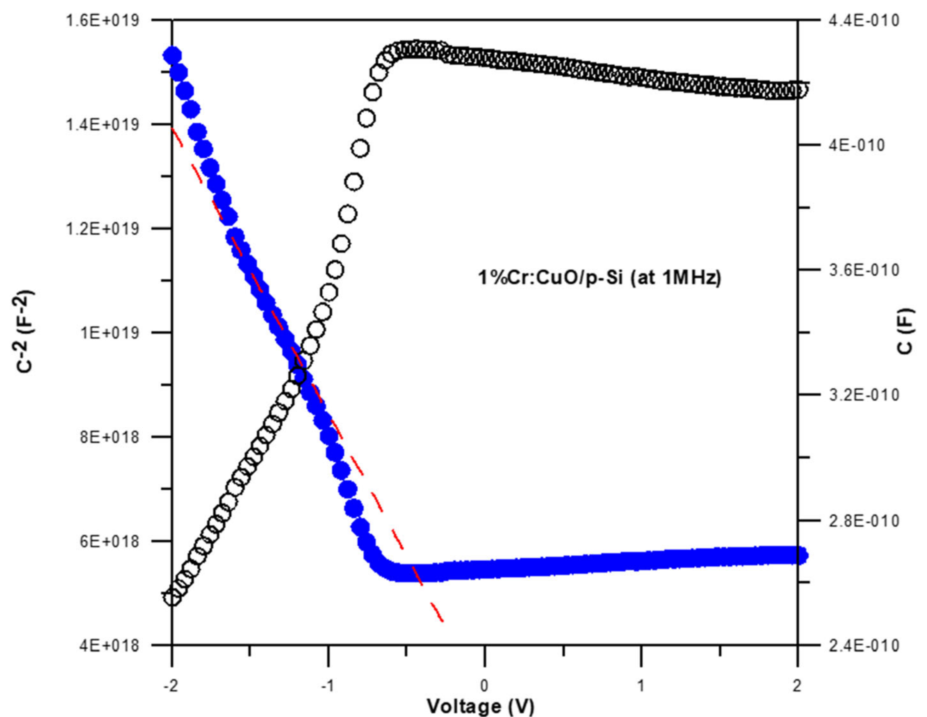

Fig. 9 C^2–*V* and *C*–*V* plots of 1%Cr:CuO/p-Si heterojunctions at 1 MHz

Author contributions

All authors contributed to the study conception and design. Material preparation, data collection, and analysis were performed by SB, IC, and CO. The first draft of the manuscript was written by SB and all authors commented on the previous versions of the manuscript. All authors read and approved the final manuscript.

Funding

The authors declare that no funds, grants, or other support were received during the preparation of this manuscript.

Data availability

The data that support the findings of this study are available from the corresponding author, IC, upon reasonable request.

Declarations

Conflict of interest The authors have no relevant financial or non-financial interests to disclose.

References

1. B.J. Hansen, N. Kouklin, G. Lu, I.-K. Lin, J. Chen, X. Zhang, J. Phys. Chem. **114**, 2440 (2010)
2. F. Bayansal, S. Kahraman, G. Çankaya, H. Çetinkara, H. Güder, H. Çakmak, J. Alloys Compd. **509**, 2094 (2011)
3. M. Rashad, M. Rüsing, G. Berth, K. Lischka, A. Pawlis, J. Nanomater. **2013**, 82 (2013)
4. A.A. Ansari, M. Alhoshan, M. Alsalhi, A. Aldwayyan, Biosensors 302 (2010)
5. A. Szkudlarek, K. Kollbek, S. Klejna, A. Rydosz, Mater. Res. Express **5**, 126406 (2018)
6. Q. Chen, L. Zhang, G. Chen, Anal. Chem. **84**, 171 (2012)
7. K.M. Kim, H.M. Jeong, H.R. Kim, K.I. Choi, H.J. Kim, J.H. Lee, Sensors (Switzerland) **12**, 8013 (2012)
8. S. Ruzgar et al., Appl. Phys. A **127**, 1 (2021)
9. Ö.B. Sürücü, H.H. Güllü, M. Terlemezoglu, D. Yildiz, M. Parlak, Physica B **570**, 246 (2019)
10. T. Viet Pham, M. Rao, P. Andreasson, Y. Peng, J. Wang, K. Jinesh, Appl. Phys. Lett. **102**, 032101 (2013)
11. M. Heinemann, B. Eifert, C. Heiliger, Phys. Rev. B **87**, 115111 (2013)
12. N. Serin, T. Serin, Ş Horzum, Y. Çelik, Semicond. Sci. Technol. **20**, 398 (2005)
13. S. Mridha, D. Basak, Semicond. Sci. Technol. **21**, 928 (2006)
14. T. Ishihara, M. Higuchi, T. Takagi, M. Ito, H. Nishiguchi, Y. Takita, J. Mater. Chem. **8**, 2037 (1998)
15. B.S. Kang et al., Adv. Mater. **20**, 3066 (2008)
16. S.K. Kumar, S. Suresh, S. Murugesan, S.P. Raj, Sol. Energy **94**, 299 (2013)
17. V. Ramya, K. Neyvasagam, R. Chandramohan, S. Valanarasu, A.M.F. Benial, J. Mater. Sci.: Mater. Electron. **26**, 8489 (2015)
18. Y.S. Chaudhary, S.A. Khan, C. Tripathi, R. Shrivastav, V.R. Satsangi, S. Dass, Nucl. Instrum. Methods Phys. Res. B **244**, 128 (2006)
19. L.-C. Chen, C.-C. Chen, K.-C. Liang, S.H. Chang, Z.-L. Tseng, S.-C. Yeh, C.-T. Chen, W.-T. Wu, C.-G. Wu, Nanoscale Res. Lett. **11**, 402 (2016)
20. D.P. Dubal, G.S. Gund, R. Holze, H.S. Jadhav, C.D. Lokhande, C.-J. Park, Dalton Trans. **42**, 6459 (2013)
21. K. Mageshwari, R. Sathyamoorthy, Mater. Sci. Semicond. Process. **16**, 337 (2013)
22. N. Mukherjee, B. Show, S.K. Maji, U. Madhu, S.K. Bhar, B.C. Mitra, G.G. Khan, A. Mondal, Mater. Lett. **65**, 3248 (2011)
23. S.C. Ray, Sol. Energy Mater. Sol. Cells **68**, 307 (2001)
24. N.A.M. Shanid, M.A. Khadar, Thin Solid Films **516**, 6245 (2008)
25. M.F. Al-Kuhaili, Vacuum **82**, 623 (2008)
26. S.H. Wee, P.-S. Huang, J.-K. Lee, A. Goyal, Sci. Rep. **5**, 16272 (2015)
27. V. Figueiredo, E. Elangovan, G. Gonçalves, P. Barquinha, L. Pereira, N. Franco, E. Alves, R. Martins, E. Fortunato, Appl. Surf. Sci. **254**, 3949 (2008)
28. H.S. Kim, J.W. Lim, S.J. Yun, M.A. Park, S.Y. Park, S.E. Lee, H.C. Lee, Jpn. J. Appl. Phys. **52**, 10MB17 (2013)
29. P. Cova, A. Singh, Solid State Electron. **33**, 11 (1990)
30. Ş Karataş, Ş Altindal, Solid State Electron. **49**, 1052 (2005)
31. S. Bhuvaneshwari, N. Gopalakrishnan, J. Alloys Compd. **654**, 202 (2016)
32. B. Gu, S. Maekawa, AIP Adv. **7**, 055805 (2017)
33. S.G. Yang, A.B. Pakhomov, S.T. Hung, C.Y. Wong, Appl. Phys. Lett. **81**, 2418 (2002)
34. S. Yilmaz, M. Parlak, S. Özcan, M. Altunba, E. McGlynn, E. Bacaksiz, Appl. Surf. Sci. **257**, 9293 (2011)
35. C. Guillén, J. Herrero, J. Alloys Compd. **737**, 718 (2018)
36. P. Samarasekara, P. Karunarathna, H. Weeramuni, C. Fernando, Mater. Res. Express. **5**, 066418 (2018)
37. M. Shaban, K. Abdelkarem, A.M. El Sayed, Phase Transit. **92**, 347 (2019)

38. S. Pat, R. Mohammadigharehbagh, C. Musaoğlu, S. Özen, Ş Korkmaz, Optik **180**, 350 (2019)
39. C.R. Gobbiner, A.M. Ali, D. Kekuda, J. Mater. Sci.: Mater. Electron. **26**, 9801 (2015)
40. S. Visalakshi, R. Kannan, S. Valanarasu, H.-S. Kim, A. Kathalingam, R. Chandramohan, Appl. Phys. A **120**, 1105 (2015)
41. S. Baturay, A. Tombak, D. Kaya, Y.S. Ocak, M. Tokus, M. Aydemir, T. Kilicoglu, J. Sol–Gel Sci. Technol. **78**, 422 (2016)
42. F. Gao, X.-J. Liu, J.-S. Zhang, M.-Z. Song, N. Li, J. Appl. Phys. **111**, 084507 (2012)
43. F.A. Akgul, G. Akgul, N. Yildirim, H.E. Unalan, R. Turan, Mater. Chem. Phys. **147**, 987 (2014)
44. P. Venkateswari, P. Thirunavukkarasu, M. Ramamurthy, M. Balaji, J. Chandrasekaran, Optik **140**, 476 (2017)
45. P. Samarasekara, N. Kumara, N. Yapa, J. Phys.: Condens. Matter **18**, 2417 (2006)
46. J. Shaikh, R. Pawar, R. Devan, Y. Ma, P. Salvi, S. Kolekar, P. Patil, Electrochim. Acta **56**, 2127 (2011)
47. D.P. Joseph, C. Venkateswaran, S. Sambasivam, B.C. Choi, J. Korean Phys. Soc. **61**, 449 (2012)
48. A. Yildiz, Ş Horzum, N. Serin, T. Serin, Appl. Surf. Sci. **318**, 105 (2014)
49. Y. Wang, T. Jiang, D. Meng, D. Wang, M. Yu, Appl. Surf. Sci. **355**, 191 (2015)
50. J. Tamaki, K. Shimanoe, Y. Yamada, Y. Yamamoto, N. Miura, N. Yamazoe, Sens. Actuators B **49**, 121 (1998)
51. H.Y. Bae, G.M. Choi, Sens. Actuators B **55**, 47 (1999)
52. Y.S. Chaudhary, A. Agrawal, R. Shrivastav, V.R. Satsangi, S. Dass, Int. J. Hydrogen Energy **29**, 131 (2004)
53. J. Morales, L. Sanchez, F. Martin, J. Ramos-Barrado, M. Sanchez, Thin Solid Films **474**, 133 (2005)
54. L. Obulapathi, A.G. Kumar, T.S. Sarmash, T.S. Rao, Int. J. Nanotechnol. **4**, 29 (2014)
55. B.D. Cullity, *Elements of X-ray Diffraction* (Addison-Wesley Publishing, Reading, 1956)
56. G. Durai, P. Kuppusami, S. Arulmani, S. Anandan, S. Khadeer Pasha, S. Kheawhom, Int. J. Energy Res. **45**(14), 20001 (2021)
57. S. Manjunatha, R.H. Krishna, T. Thomas, B. Panigrahi, M. Dharmaprakash, Mater. Res. Bull. **98**, 139 (2018)
58. S. Dolai, R. Dey, S. Das, S. Hussain, R. Bhar, A. Pal, J. Alloys Compd. **724**, 456 (2017)
59. A. Menazea, A.M. Mostafa, J. Environ. Chem. Eng. **8**, 104104 (2020)
60. J. Tauc, *Amorphous and Liquid Semiconductors* (Springer Science & Business Media, Berlin, 2012)
61. M.A. Green, Sol. Energy Mater. Sol. Cells **92**, 1305 (2008)
62. Y. Gülen, F. Bayansal, B. Şahin, H.A. Çetinkara, H.S. Güder, Ceram. Int. **39**, 6475 (2013)
63. M. Sajid, M. Imran, Salahuddin, J. Iqbal, Appl. Phys. A **124**, 768 (2018)
64. M.R. Das, P. Mitra, J. Sol–Gel Sci. Technol. **87**, 59 (2018)
65. G.Y. Naser, W.N. Raja, A.S. Faris, Z.J. Rahem, M.A. Salih, A.H. Ahmed, Energy Procedia **36**, 42 (2013)
66. C. Coşkun, H. Güney, E. Gür, S. Tüzemen, Turk. J. Phys. **33**, 49 (2009)
67. Y. Caglar, M. Caglar, S. Ilican, F. Yakuphanoglu, Microelectron. Eng. **86**, 2072 (2009)
68. S.M. Sze, Y. Li, K.K. Ng, *Physics of Semiconductor Devices* (Wiley, Amsterdam, 2021)
69. B. Gunduz, I. Yahia, F. Yakuphanoglu, Microelectron. Eng. **98**, 41 (2012)
70. K. Akkiliç, A. Türüt, G. Çankaya, T. Kiliçoğlu, Solid State Commun. **125**, 551 (2003)
71. A. Yeşildağ, M. Erdoğan, Ö. Sevgili, Z. Çaldıran, İ Orak, J. Electron. Mater. **50**, 6448 (2021)
72. A. Karabulut, H. Efeoglu, A. Turut, J. Semicond. **38**, 054003 (2017)
73. S. Ruzgar, S.A. Pehlivanoglu, Superlattices Microstruct. **145**, 106636 (2020)
74. İY. Erdoğan, Ö. Güllü, J. Alloys Compd. **492**, 378 (2010)
75. R. Tung, Phys. Rev. B **45**, 13509 (1992)
76. S. Ruzgar, Y. Caglar, O. Polat, D. Sobola, M. Caglar, Surf. Interfaces **21**, 100750 (2020)
77. Ç. Bilkan, S. Zeyrek, S. San, Ş Altındal, Mater. Sci. Semicond. Process. **32**, 137 (2015)
78. R. Singh, L. Yadav, T. Shweta, Thin Solid Films **685**, 195 (2019)
79. H. Norde, J. Appl. Phys. **50**, 5052 (1979)
80. Ö. Güllü, T. Kilicoglu, A. Türüt, J. Phys. Chem. Solids **71**, 351 (2010)
81. V.R. Reddy, Thin Solid Films **556**, 300 (2014)
82. O. Dayan, A.G. Imer, M. Tercan, A. Dere, A.G. Al-Sehemi, A.A. Al-Ghamdi, F. Yakuphanoglu, J. Mol. Struct. **1238**, 130464 (2021)
83. Ö. Güllü, S. Asubay, Ş Aydoğan, A. Türüt, Physica E **42**, 1411 (2010)
84. H. Aydin, A. Tataroğlu, A.A. Al-Ghamdi, F. Yakuphanoglu, F. El-Tantawy, W. Farooq, J. Alloys Compd. **625**, 18 (2015)
85. S. Baturay, Y.S. Ocak, D. Kaya, J. Alloys Compd. **645**, 29 (2015)
86. E.H. Rhoderick, IEE Proc. I Solid State Electron Devices **129**, 1 (1982)

Publisher's Note Springer Nature remains neutral with regard to jurisdictional claims in published maps and institutional affiliations.